IMAGE ANALYSIS USING THE RANDOM-DOT SCREEN MODEL: THE METHOD AND RESULTS

K.I.Voliak, K.A. Boyarchuk and A.V.Krasnoslobodtsev
General Physics Institute of the USSR Ac.Sci.
38 Vavilov street, 117942 Moscow, USSR, Commission IV

ABSTRACT. One of the classical problems on random screen diffraction is considered, where (non)transparent apertures are dispersed over a dark (transparent) screen. The analytical result is to determine an aperture dimension variance and other image statistical parameters by using the Fourier transform. The simulated and actual images are optically processed, thereby confirming the theory developed.

1. INTRODUCTION. The mathematical aspect of image analysis involving some integral, for example, Fourier transform is often very similar to the known theoretical problem on interaction between a coherent electromagnetic wave and a random screen or another randomly inhomogeneous medium. The general solution to the problem is rather bulky [1]. Various simplified models of random screens have been developed for atmospheric remote sensing [2] and statistical optics [3]. In this paper we consider some special model of random-screen light diffraction and apply it to the image processing so as to determine statistical parameters of actual images.

2. RANDOM-DOT SCREEN MODEL. In many cases we deal with an image consisting of dark (or bright) spots of some regular form dispersed rather uniformly against a very bright (or dark) background. The simplest situation is a two-level image of partially transparent round apertures, which are randomly distributed over a rectangular and totally impermeable screen. Let an aperture ensemble be a realization of the probability process in which the central coordinates and the radii of apertures are random quantities.

In the Fourier-lens focal plane of a coherent optical analyzer we usually observe the intensity of light waves passing through the image transparency, namely, we take the squared Fourier-transform modulus $|F|^2$ of the transparency function f. The latter is a local transparency 1_n within each aperture of the number n and the square S_n, with $^n f=0$ on the outerside of S_n. For the sake of definiteness, we assume that the probability of aperture overlapping is negligible. Then, the Fourier transform of all N apertures of the image transparency is

$$F(f) = \sum_{n=1}^{N} 1_n \iint_{S_n} \exp(ik_1 x + ik_2 y)dx\,dy , \qquad (1)$$

where $S_n = \{(x-a_n)^2 + (y-b_n)^2 = r_n^2\}$; r_n, a_n and b_n are the radius and the coordinates of an aperture in the image plane (x,y), respectively; (k_1, k_2) are the coordinates in the Fourier plane.

In the reference frame of each aperture ($x' = x-a_n$, $y' = y-b_n$), we can rewrite (1) in the form:

$$F(f) = \sum_{n=1}^{N} l_n \exp(ik_1 a_n + ik_2 b_n)\left[\iint_{S_n'} \exp(ik_1 x' + ik_2 y')dx'dy'\right], \quad (2)$$

where $S_n' = (x'^2 + y'^2 = r_n^2)$.
Here we know that the inner integral in (2) is the obvious relation for the Fraunhofer diffraction from a round diaphragm

$$K_n = \iint_{S_n} \exp(ik_1 x' + ik_2 y')dx'dy' = \frac{2\pi r_n}{\sqrt{k_1^2 + k_2^2}} J_1\left(r_n \sqrt{k_1^2 + k_2^2}\right), \quad (3)$$

which is homogeneous in the Fourier plane due to the homogeneity of the first-order Bessel function $J_1(.)$ of real arguments.

For the sake of simplicity, let all apertures have the same transparency $l_n = 1$. Then, collecting the terms of (2), which are dependent on the aperture radii, into a separate sum, we have

$$F(f) = \frac{2\pi l}{k} \exp(ik_1 \bar{a} + ik_2 \bar{b}) \sum_{n=1}^{N} r_n J_1(k r_n), \quad (4)$$

where $k = (k_1^2 + k_2^2)^{1/2}$, $\bar{a}$ and $\bar{b}$ are certain average coordinates of aperture centers (a_n, b_n). A detailed account of the exponents of (2) will be taken separately.

For a fairly large statistical sample, we can replace summation (4) by the integration over the probability density $W(r)$ of the aperture radius distribution,

$$\sum_{n=1}^{N} r_n J_1(k r_n) \rightarrow N \int_0^{\infty} r W(r) J_1(kr)dr. \quad (5)$$

Therefore, the mean light intensity in the focal plane, i.e. the average Wiener spectrum, is equal to

$$\langle |F(f)|^2 \rangle = \frac{4\pi^2 l^2}{k^2} N^2 \left(\int_0^{\infty} r W(r) J_1(kr)dr\right)^2. \quad (6)$$

3. SPECTRA AS DEPENDENT ON THE RADIUS DISTRIBUTION. Calculus of (6) requires, in general, a lengthy algebra. For instance, let the probability density be a universal one-peak function

$$W(r) = C r^{\beta-1} e^{\alpha r}, \quad (7)$$

where α and β are some free constants, while the normalizing constant C is defined by $\int_0^{\infty} W(r)\,dr = 1$: $C = \alpha^{\beta}/\Gamma(\beta)$, $\Gamma(.)$ is the gamma function. Then, the integral $I = \int_0^{\infty} r W(r) J_1(kr)dr$ equals

$$I = \frac{\Gamma(\beta+2)}{\Gamma(\beta)} P_{\beta}^{-1}(\alpha / \sqrt{\alpha^2 + k^2}) , \qquad (8)$$

where $P_{\beta}^{-1}(.)$ is the first-kind associated Legendre function for negative arguments. With due account of the gamma-function properties, Wiener spectrum (6) is

$$\langle |F(f)|^2 \rangle = 4\pi^2 l^2 N^2 \frac{\beta^2(\beta+1)^2\alpha^{2\beta}}{k^2(\alpha^2+k^2)^{\beta+1}} (P_{\beta}^{-1}(\alpha / \sqrt{\alpha^2+k^2}))^2. \qquad (9)$$

In the simplest case $\beta = 1$, we have

$$\langle |F(f)|^2 \rangle = 4\pi^2 l^2 N^2 \alpha^4 (\alpha^2 + k^2)^{-3}. \qquad (10)$$

It is clear from (10) that there are no spectrum intensity maxima for a rather 'flat' probability density W(r).

If we are interested in some small typical difference $k\Delta r_n = k(r_n - \bar{r})$, the following expansion exists :

$$J_1(kr) = J_1(k\bar{r}) + k\Delta r_n \left.\frac{dJ}{dz}\right|_{z=k\bar{r}} + \frac{1}{2}(k\Delta r_n)^2 \left.\frac{d^2J}{dz^2}\right|_{z=k\bar{r}} + \ldots \qquad (11),$$

where $\bar{r} = N^{-1}\sum_{n=1}^{N} r_n$ is the average empirical radius and, hence, the linear term in (11) is zero. In addition, the cubic terms in (11) are alternating quantities and in our subsequent calculations we can restrict ourselves to the second-order accuracy $O((k\Delta r_n)^2)$.

Let us consider the summation

$$\sum_{n=1}^{N} r_n J_1(kr_n) \approx N\bar{r} J_1(k\bar{r}) + \left(\sum_{n=1}^{N} (\Delta r_n)^2\right)\left(k\left(J_0 - \frac{J_1}{k\bar{r}}\right) + \frac{k^2\bar{r}}{2}\left[\left(\frac{2}{k^2\bar{r}^2} - 1\right)J_1 - \frac{J_0}{k\bar{r}}\right]\right)_{z=k\bar{r}}. \qquad (12)$$

Introducing the empirical radius variance $D_2 = N^{-1}\sum_{n=1}^{N}(\Delta r_n)^2$, we rewrite (12) in the form:

$$\sum_{n=1}^{N} r_n J_1(kr_n) = N\bar{r} J_1(k\bar{r}) + N\frac{D_2}{2}[kJ_0(k\bar{r}) - k^2\bar{r}J_1(k\bar{r})]. \qquad (13)$$

Finally, the total mean Wiener spectrum is

$$\langle |F(f)|^2 \rangle = \frac{4\pi^2 l^2 N^2}{k^2}\left(\bar{r}J_1(k\bar{r}) + \frac{D_2}{2}[kJ_0(k\bar{r}) - k^2\bar{r}J_1(k\bar{r})]\right)^2. \qquad (14)$$

As seen from (14), the radius variance, as well as other high momenta, distort markedly conventional diffraction (3).

4. COMPLEX SPECTRAL COMPONENTS. The exponents of (2), which

are dependent on the coordinates and are independent of the radii, will be singled out into a common sum:

$$F(f) = \frac{2\pi l}{k} \bar{N} \bar{r} J_1(k\bar{r}) \sum_{n=1}^{N} \exp(ik_1 a_n + ik_2 b_n). \qquad (15)$$

To account for the regular complex spectral component of the uniform distribution of apertures, we suggest that the apertures are placed at the knots of a rectangular grid:

$$G = \sum_{n=1}^{N} \exp(ik_1 a_n + ik_2 b_n) = \sum_{p=1}^{N} e^{ik_1 ph} \sum_{q=1}^{N} e^{ik_2 qs}, \qquad (16)$$

where N_1 and N_2 are the numbers of knots on the two grid sides ($N_1 \times N_2 = N$), h and s are the grid constants in mutually orthogonal directions. Calculus of (16) yields

$$G(k_1, k_2) = \frac{\sin(\frac{N_1+1}{2} k_1 h) \sin(\frac{N_2+1}{2} k_2 s)}{\sin\frac{k_1 h}{2} \sin\frac{k_2 s}{2}}, \qquad (17)$$

It is evident from (17) that in the spectrum there arises a reciprocal rectangular grid having a very bright central spot. For an isotropic sguare screen, where $k_1, k_2 \to k$, $N_1 = N_2 = \sqrt{N}$, the grid steps h,s tend to the mean spacing $\bar{h}$.

To illustrate the effect of random deviation $\Delta a_n, \Delta b_n$ from the regular-grid knots, we can consider, for the sake of simplicity, a one-dimensional randomly distorted grid:

$$\sum_{p=1}^{\sqrt{N}} e^{ika_p} = \sum_{p=1}^{\sqrt{N}} \exp ik(ph+\Delta a_p) = \sum_{p=1}^{N} e^{ikph}[1 + ik\Delta a_p - \frac{k}{2}(\Delta a_p)^2 + \ldots]. \qquad (18)$$

Proceeding to empirical statistical momenta and omitting odd expansion terms, we find that

$$\sum_{p=1}^{N} e^{ika_p} = G(k)[1 - \frac{k^2}{2}\langle(\Delta a_p)^2\rangle + \frac{k^4}{12}\langle(\Delta a_p)^4\rangle + \ldots], \qquad (19)$$

where $G(k) = \dfrac{\sin\frac{\sqrt{N}+1}{2} kh}{\sin\frac{kh}{2}}$.

Relation (19) demonstrates clearly that the spectral envelope may be highly modulated at finite values $\langle(\Delta a_p)^2\rangle$ and higher momenta. The above consideration also remainsvalid for random deviations Δb_q. Here one can consider that $\langle(\Delta a_p^2)\rangle^{1/2} = \langle(\Delta b_q^2)\rangle^{1/2} = (\bar{h} - 2\bar{r})/2$. Thus, the final Wiener spectrum of our model image is

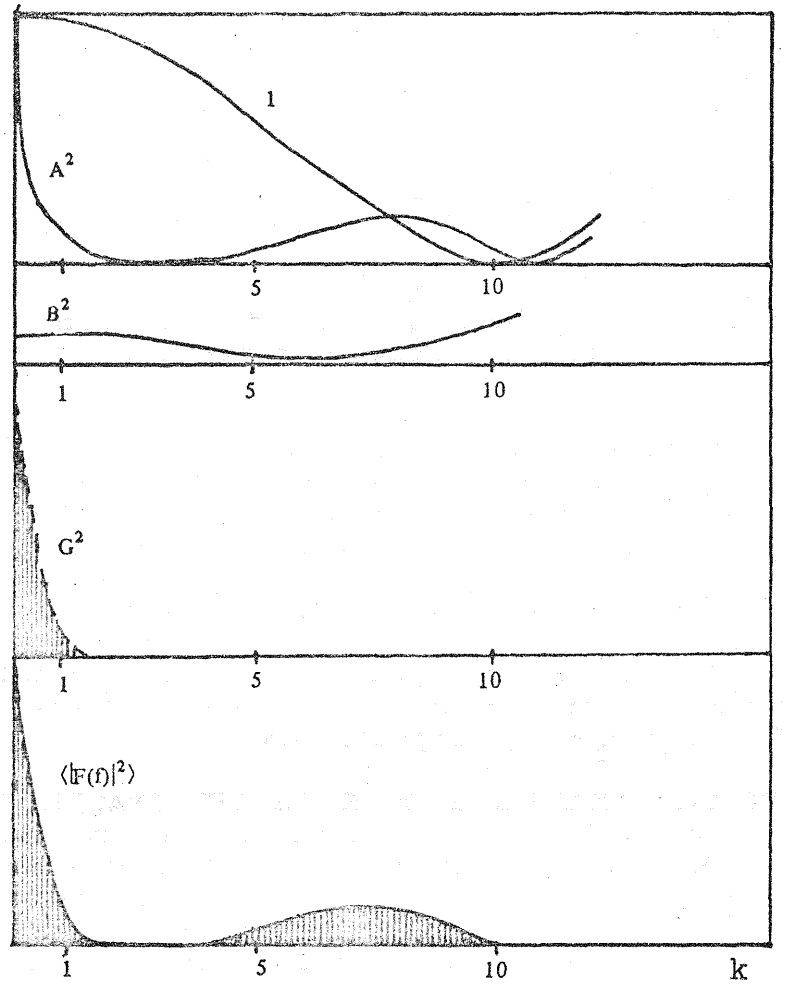

Fig.1. Formation of spectrum (20)

Fig.2. Poor sample of small apertures d_1 (a) and its spectrum (b)

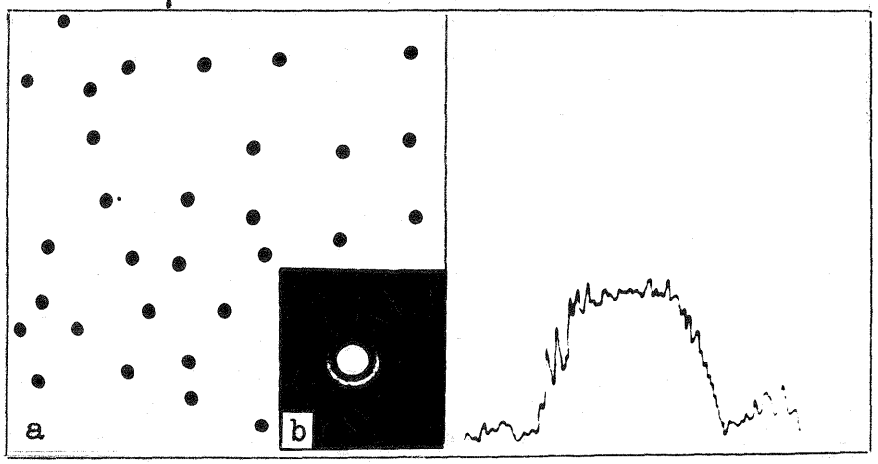

$$\langle |F(f)|^2 \rangle = \frac{4\pi^2 l^2 N^2}{k^2} G^2(k)[\bar{r}J_o(k\bar{r}) + A]^2(1 - B)^4 , \qquad (20)$$

where

$$A = \frac{D^2}{2}[KJ(k\bar{r}) - k^2\bar{r}J_1(k\bar{r})]^2$$

is the sum of terms describing the aperture radius distribution,

$$B = [-\frac{k^2}{2}\langle(\Delta a_\rho)^2\rangle + \frac{k^4}{12}\langle(\Delta a_\rho)^4\rangle$$

is the analogous sum for their spacing distribution, $G^2(k)$ is the coefficient defining a speckle structure of the Fourier transform.

We assume the interdependence of the various random quantities considered to be negligible. The shape of final spectrum (20) is explained by the graph of Fig. 1 plotted for small k, $0 < k \leq 10$. Fig. 1 presents : (i) the undisturbed spectrum $M_o \propto \bar{r} J_o(k\bar{r})$ of the averaged aperture; (ii) the spectrum modulation $M_1 = [\bar{r}J_o(k\bar{r}) + A]^2$ by radius statistics; (iii) the additional modulation $M_2 = (1 - B^4)$ by complex spectral components ; (iv) the high-frequency content $M_3 = G^2(k)$, i.e. the speckle structure of the spectrum; and (v) the resulting spectrum $\langle |F|^2 \rangle = M_o M_1 M_2 M_3$, respectively.

5. COHERENT OPTICAL PROCESSING OF SIMULATED IMAGES. To verify our model we have utilized the conventional optical Fourier processor [4]. A He-Ne laser of wavelength 632.8 nm was used as a source of coherent light. The Fourier lens was 180 mm in diameter and had a focal distance of 3.7 m. We used also an immersion cell to avoid phase distortions introduced by a transparency photofilm. The resulting errors of establishing spatial spectral freguencies were around three per cent, while those in spectral intensity measurements were defined by spectral speckles and were around ten per cent.

We have been able to preparate special images proximating fairly well the developed mathematical model and then we succeeded in their optical processing. The image transparencies and their spectra are presented in Figs.2 through 5. Here one can see two sorts of round transparent apertures with diameters $d_1 = 2.25 \pm 0.05$ and $d_2 = 4.35 \pm 0.05$ mm, respectively, which are distributed rather irregularly over an impermeable square screen.

The spectrum of a poor sample of the small apertures d_1 (Fig. 2) is virtually identical to the Fraunhofer diffraction from a single round aperture and the spectral intensity level is close to that of (3) . Meanwhile the spectrum of a more representative sample of d_1 (Fig.3) is, in general, analogous to that of Fig.2 although it is notable for some peculiarities. Namely, the former consists of distinct random speckles, as predicted by the theoretical term M_3, and its central peak is split by the radius modulation M_1. Figs.4 and 5 show the scale transform of images; for example, the spectrum of the apertures, d_2 (Fig.4) is uniformly contracted in comparison to that of Fig.2. The image of Fig.5 contains apertures of the two diameters, as the limiting case of random-radius

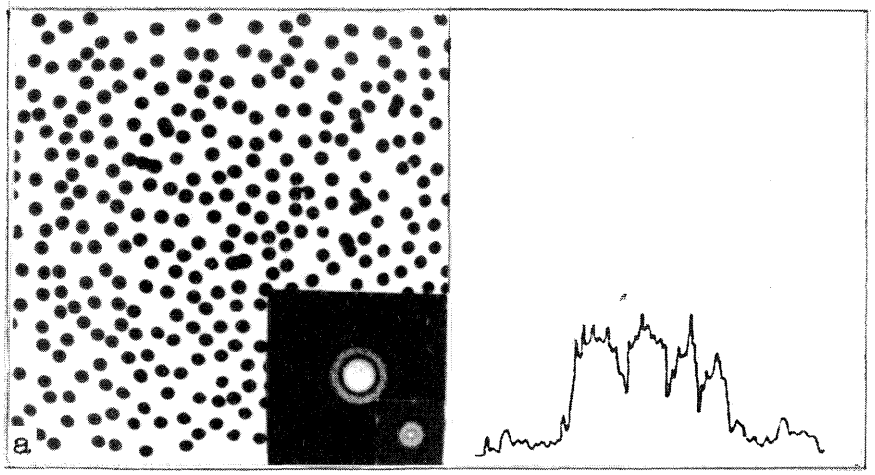

Fig.3. More representative sample of d_1 and its spectrum

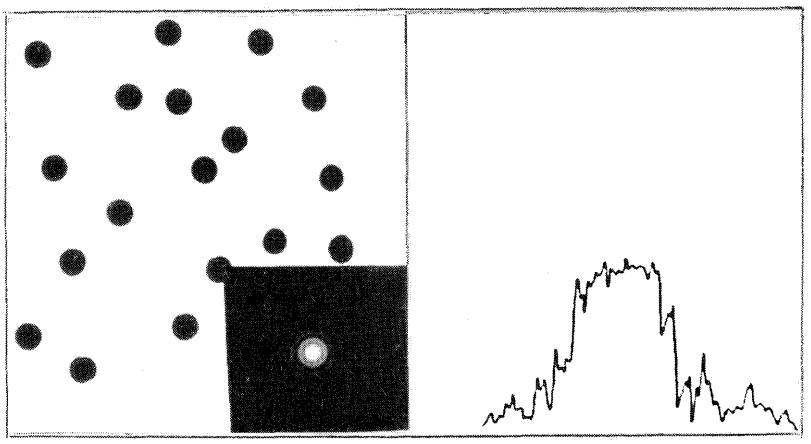

Fig.4. Scale transform of image and spectra: a sample of d_2

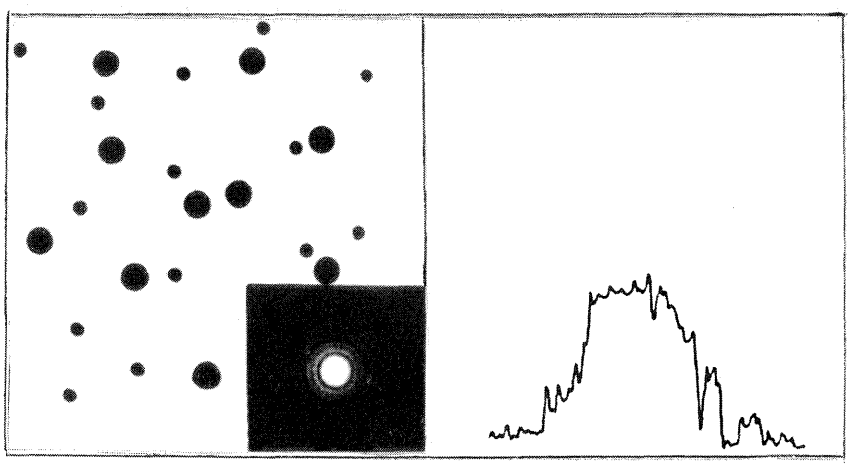

Fig.5. Apertures of the two diameters

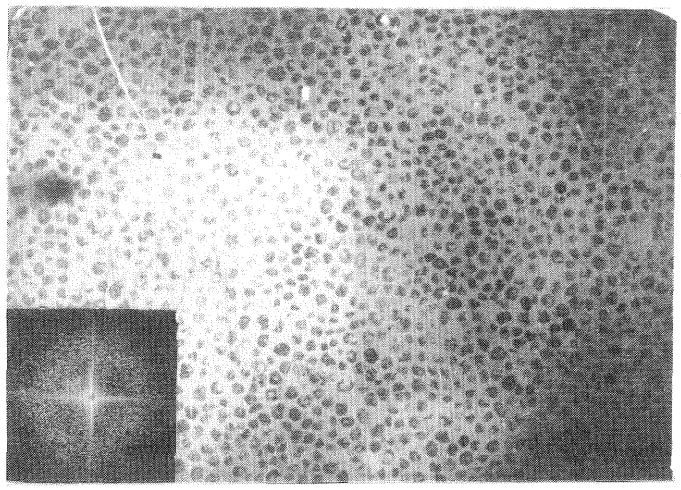

Fig.6. Actual photodraphic image and its spectrum

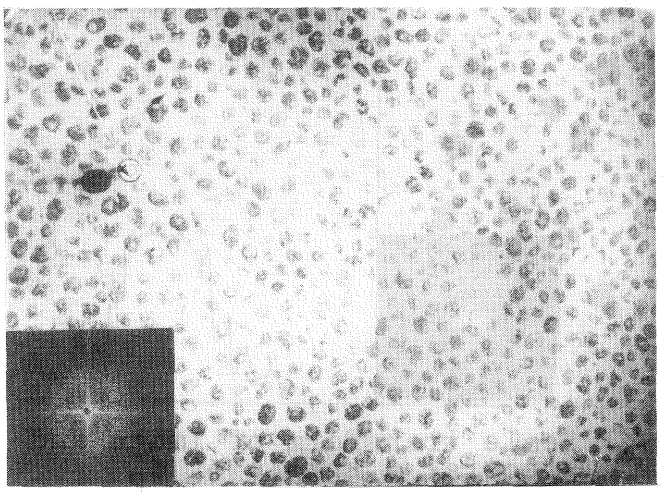

Fig.7. Actual image with a lag among concretions

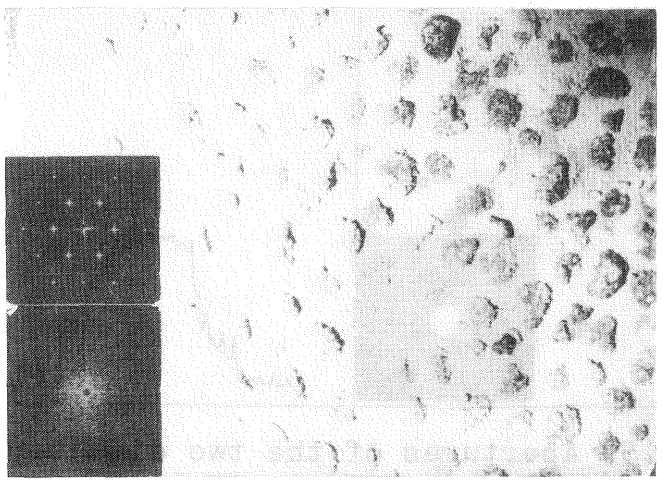

Fig.8. Actual image: a scale spectrum

modulation giving rise to a double set of spectral rings.

6. SPECTRAL ANALYSIS OF ACTUAL UNDERWATER IMAGES. Our theoretical model fits very well the actual photographic images (Figs. 6a-8a) of an ocean bottom covered by ferro-manganic concretions. In Fig. 7a one can distinctly see a round lag among concretions, that may be used for image scaling. Figs. 6b-8b show spectra of the bottom images, while Fig. 8b also gives a scale-grid spectrum. All the spectra, as a whole, are speckled round spots of higher intensity at their periphery. The central sharp peak in the spectra has been additionally screened for the sake of better presentation. The specific 'cross' in the spectra is the effect of diffraction from the boundaries of rectangular images. Fig.9 plots the photometric density of the spectrum of Fig. 6b, averaged over an angle of 15° along the 45°- direction with the vertical. The intensity 'dip' in the middle of the plot results from the above-mentioned additional screen.

The model developed here predicts that the spectrum lies in the central Airy area of the mean-radius aperture (concretion). The shortage of intensity of wavenumbers near the half-diameter of the spectrum is, primarily, a statistical effect of variations in concretion dimensions and spacings. But the former effect is relatively weaker because, even at highly variable radii $r_{min} \leqslant r \leqslant r_{max} = 2r_{min}$, the value of k^2D^2, responsible for the random modulation M_1, does not exceed $k^2r^2/9$. Meanwhile, under the actual condition $\bar{h} = 4\bar{r}$, the random modulation M_2 by concretion spacings is approximately proportionall to $k^2r^2 >> k^2r^2/9$. In general, our model may be helpful to elaborate various numerical algorithms to be used for determining the variances of concretion dimensions and spacings.

Practically, coherent optical processing may establish the capacity of minerals in an interrogated area of the ocean bottom. Using the grid spectrum (Fig. 8b) and the lag scale (Fig. 7a) we readily define the most probable dimensions of concretions. Assuming that the latter are spherical in the form and calculating their mean number over a certain specific area, we establish the total mass of a mineral lying on this site of the sea bottom.

7. CONCLUSIONS We have developed a statistical mathematical model of light diffraction from a nontransparent screen randomly covered by transparent apertures. The contribution of random variations in the aperture diameters and spacings has been determined, which strongly affects the Fourier spectra, as compared to the conventional diffraction from a single round aperture. The theoretical conclusions have been verified experimentally by means of simulated random screens used as transparencies in a laser Fourier processor. Finally, we have suggested and realized a method for determining the dimensions of ferro-manganic concretions on the basis of a coherent optical analysis of sea-bottom photoimages.

REFERENCES

1. Born M. and Wolf E. Principles of Optics. Lond.-N.Y., 1964.

2. Shifrin K.S. Light Scattering in a Muddy Medium. Gostekhizdat, Moscow, 1951.

3. DeWitt C., Blandin A. and Cohen-Tannoudji C., Eds. Quantum Optics and Electronics. N.Y., Gordon and Breach, 1965.

4. Goodman J.W. Introduction to Fourier Optics. McGraw-Hill, N.Y., 1968.

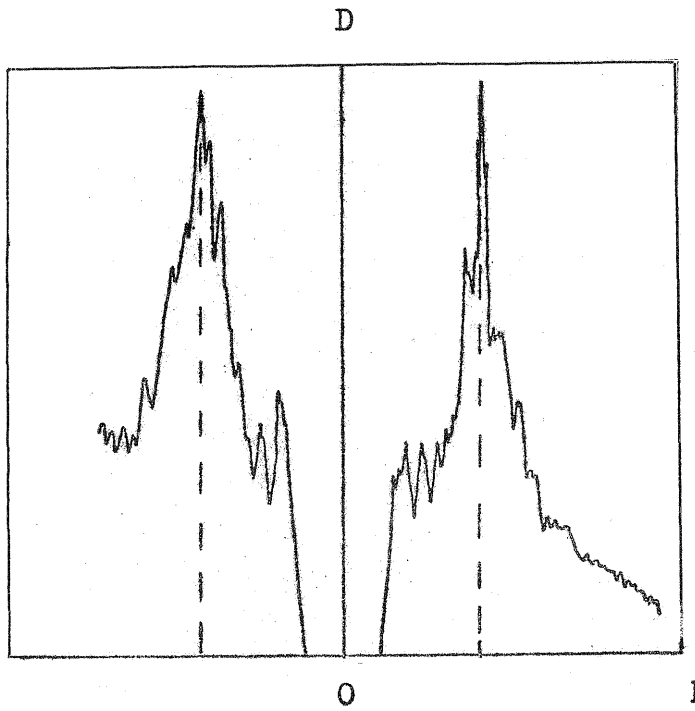

Fig.9. Photometric density of the spectrum of Fig.6